Entropy, vortex interactions, and the phase diagram of heavy-ion-irradiated $Bi_2Sr_2CaCu_2O_{8+\delta}$

C. J. van der Beek and M. Konczykowski

Laboratoire des Solides Irradiés, CNRS UMR 7642, Ecole Polytechnique, 91128 Palaiseau, France

R. J. Drost and P. H. Kes

Kamerlingh Onnes Laboratorium, Leiden University, P.O. Box 9506, 2300 RA Leiden, The Netherlands

N. Chikumoto

Superconductivity Research Laboratory, ISTEC, Minato-ku, Tokyo 105, Japan

S. Bouffard

Centre Interdisciplinaire de Recherche avec les Ions Lasers (CIRIL), Boîte Postale 5133, 14040 Caen Cedex, France

Dynamic and thermodynamic magnetization experiments on heavy-ion-irradiated single-crystalline $Bi_2Sr_2CaCu_2O_{8+\delta}$ are correlated in order to clarify the nature of the mixed-state phase diagram. It is shown that whereas the entropy contribution to the free energy in the London regime plays a minor role in unirradiated crystals and irradiated crystals at fields close to or above the matching field B_ϕ, it becomes very important at low fields in irradiated crystals with high B_ϕ. The direct determination of the entropy contribution to the free energy from the reversible magnetization allows one to determine not only the correct values of the pinning energy, but also to extract quite detailed information on pancake vortex alignment. The characteristic field $H_{int} \sim \frac{1}{6}B_\phi$ at which intervortex repulsion begins to determine the vortex arrangement and the reversible magnetization is shown to coincide with a sharp increase in the irreversibility field $H_{irr}(T)$ and with the recoupling transition found in Josephson plasma resonance. Above H_{int}, the repulsive interaction between vortices causes both the vortex mobility to decrease and pancake alignment to increase. At higher fields $\gtrsim \frac{1}{3}B_\phi \gg B_{c1}$, free vortices outnumber those that are trapped on a columnar defect. This causes the decrease of the c-axis resistivity and a second crossover of the irreversibility field, to a regime where it is determined by plastic creep.

I. INTRODUCTION

The remarkable influence of heavy-ion-irradiation-induced amorphous columnar defects on the mixed-state phase diagram and transport properties of layered superconductors, and the interplay between the pinning of vortices and coupling between the layers, has provoked a great deal of interest.[1–13] The effect of the ion tracks is twofold. First, the destruction of superconductivity within the columnar defect core, the radius of which is comparable to the superconducting coherence length ξ, leads to a large reduction of the mixed-state free energy[14–18] arising from the pinning of the two-dimensional pancake vortices in the superconducting layers[19,20] by the columns. The reduction in free energy due to pinning is readily measurable because it entails a significant reduction of the reversible magnetization M_{rev} at fields well below the matching field $B_\phi = \Phi_0 n_d$ and a nonmonotonicity of $\partial M_{rev}/\partial \ln B$ as a function of B ($\Phi_0 = h/2e$ is the flux quantum and n_d is the density of column intersections with the layers).[14–16] The coincidence of the radius of the columnar defect core with that of the vortex core implies a large pinning force[21] and concomitantly large values of the critical current density,[5] as well as a large increase of the field $H_{irr}(T)$ below which irreversible magnetic response is measured.[5] Second, the linear geometry of the ion tracks results in the effective alignment of the pancake vortices

along the tracks and the reestablishment of interlayer superconducting phase coherence at temperatures and fields where the unirradiated material behaves as a stack of nearly decoupled superconducting layers.[4,7,22–25] The pancake vortex alignment is manifest in the angular dependence of the transport properties of the irradiated superconductor,[4,6] as well as in measurements of the c-axis conductivity (perpendicular to the superconducting layers) (Refs. 9, 10, 26, and 27) and of the field at which the Josephson plasma resonance occurs in the range 24–45 GHz.[11,12,28,29] Measurements of the Josephson plasma resonance and of the c-axis conductivity,[26,27] which have the advantage of directly probing the Josephson critical current and the cosine of the average phase difference between layers, show the existence, in the heavy-ion-irradiated layered superconductor $Bi_2Sr_2CaCu_2O_{8+\delta}$, of a regime $B_l(T) < B < B_h(T)$ in the vortex liquid state in which interlayer superconducting phase coherence increases as the magnetic field is increased (i.e., a ''recoupling''). This behavior is qualitatively opposite to that found in the unirradiated material. At fields greater than B_h, interlayer phase coherence again decreases as field is increased.

The peculiar field dependence of the c-axis electromagnetic response, as well as that of the reversible—and even of the irreversible part of the magnetization [below $H_{irr}(T)$] (Ref. 13)—has been interpreted in terms of the competition between the Josephson coupling energy, which tends to align

pancake vortices, and the entropy contribution to the free energy arising from a random distribution of pancakes over columnar defects.[30] The importance of intralayer pancake repulsion is often downplayed, even though it has been shown to be important in determining the pancake arrangement,[31] reversible magnetization,[14,31] and transport properties.[31] It is the purpose of this paper to investigate the importance of the contributions of intra- and interlayer pancake vortex interaction energy, entropy, and pinning energy to the Gibbs free energy G and the impact of each on the phase diagram of heavy-ion-irradiated $Bi_2Sr_2CaCu_2O_{8+\delta}$. To this effect, we have performed reversible magnetization as well as ac screening measurements on heavy-ion-irradiated $Bi_2Sr_2CaCu_2O_{8+\delta}$ with widely varying matching fields (Sec. II). From the analysis presented below (Sec. III A), it turns out that in the London regime, the entropy contribution to the reversible magnetization is rather insignificant with respect to the total magnetization or its modification due to vortex pinning on the columnar defects. Only in irradiated crystals with sufficiently high B_ϕ is it essential to take a configurational entropy contribution into account when describing the magnetization and, then, only at low fields $B \ll B_\phi$ (Sec. III A 2). As a consequence, previous estimates of pinning energies[15,16,32] determined from the reversible magnetization should be revised towards (sometimes significantly) lower values. Next, it is shown how information on pancake alignment can be obtained from the reversible magnetization (Sec. III A 3). The data allow for the extraction of the field H_{int} at which vortex repulsive interactions begin to determine the pancake vortex arrangement over the columnar defects. This field correlates very well with sharp features in the irreversibility line and, in some cases, with the ''recoupling'' observed in the JPR measurements and c-axis conductivity (Sec. III B).

II. EXPERIMENTAL DETAILS

A. Sample preparation

For this study, we have used $Bi_2Sr_2CaCu_2O_{8+\delta}$ single crystals grown at the University of Amsterdam by the traveling solvent floating zone technique.[33] A number of crystals were postannealed at 800 °C in air and had $T_c = 90.0$ K. Other crystals were retained as grown—this yields samples that are lightly overdoped in oxygen, and that have $T_c \approx 83$ K. Another batch of crystals, grown at the University of Tokyo using the same technique,[34] had $T_c = 88.8$ K and was used for the measurements of the irreversibility line for different matching fields. After growth and annealing, large crystals were selected for uniformity and absence of macrodefects, and subsequently cut using a wire saw, so as to produce small squares of typical size $800 \times 800 \times 20$ μm^3, suitable for magnetometry experiments. A number of larger pieces (1×2 $mm^2 \times 20$ μm) of the Amsterdam crystals were kept for reversible magnetization measurements using a commercial superconducting quantum interference device (SQUID) magnetometer, as well as ac transmittivity measurements. In this manner, a sizable number of crystals with similar characteristics was obtained.

The samples were irradiated with 5.8 GeV Pb ions at the Grand Accélérateur National d'Ions Lourds (GANIL) at Caen, France. Such an irradiation produces continuous amorphous tracks of radius $c_0 \sim 3.5$ nm which traverse the samples along their entire thickness. During the irradiation, the ion beam traverses a 1-μm-thick Ti film placed in front of the sample; the secondary electron emission from this film is used to continuously monitor the ion flux during irradiation. At the beginning of each run, the ion flux is calibrated using a Faraday cup placed between the Ti film and the sample. This procedure allows one to accurately control the total ion fluence for each sample. Moreover, the ion beam is continuously swept across the target using asynchronous vertical (3 Hz) and horizontal (1 kHz) ac drive fields so as to expose the entire target area (2×3 cm^2) homogeneously. Different crystals from each source were irradiated with widely different ion fluences, in order to produce samples with dose equivalent matching fields 0.02 T$< B_\phi <$4 T. There was a slight reduction of the samples' T_c after the irradiation. Notably, overdoped single crystals had a T_c of 81 K and 78.7 K after irradiation to doses corresponding to $B_\phi = 2$ and 4 T, respectively. The crystals from the University of Tokyo underwent a reduction of T_c of up to 4 K (for $B_\phi = 4$ T).

B. ac shielding

The ac transmittivity[35] was measured using the Local Hall Probe Magnetometer, in the same way as described in Ref. 36. The sample was placed on top of a miniature InSb Hall sensor; both were surrounded by an ac drive coil that could produce fields h_{ac} of up to 30 G (at frequencies 0.5 Hz$< f$ <2 kHz). The ac field was always directed parallel to the sample c axis. This corresponds to the application to the sample of an azimuthal electric field E_ϕ with gradient $r^{-1}\partial(rE_\phi)/\partial r = 2\pi h_{ac}f$ (r is the radial coordinate). The ac Hall voltage V_{ac} was measured as a function of temperature and applied field H_a. From V_{ac}, the first and third harmonic components of the transmittivity are determined as

$$T_H(f,T) \equiv [V_{ac}(f,T) - V_{ac}(f,T \ll T_c)]/[V_{ac}(f,T \gg T_c) - V_{ac}(f,T \ll T_c)]$$

and

$$T_{H3} \equiv V_{ac}(3f,T)/[V_{ac}(f,T \gg T_c) - V_{ac}(f,T \ll T_c)],$$

respectively. In order to determine the irreversibility field $H_{irr}(T,f)$ [or irreversibility temperature $T_{irr}(H_a,f)$], the transmittivity was measured using an ac field of amplitude $h_{ac} = 1$ G and frequency $f = 7.75$ Hz. $T_{irr}(H_a,f)$ was taken as the temperature at which the T_{H3} signal first becomes distinguishable from the background noise when cooling. Given the size of our samples, this corresponds to probing whether the $E(j)$ characteristic deviates from Ohm's law at an electric field value of 0.6 nV cm^{-1}. In practice, the measurement of T_{irr} is often limited by instrumental resolution, which can be estimated by comparing the signal at full screening to the noise level; it corresponds, for a sample of area 800×800 μm^2, to a circulating shielding current density of 4×10^2 A m^{-2}.

C. Reversible magnetization

Measurements of the reversible magnetization were carried out using a commercial SQUID magnetometer at the University of Leiden. Care was taken to avoid the numerous artifacts previously observed in such measurements. Notably, we have found that the reported ''clockwise'' hysteresis[37] is an artifact related to the use of a too restricted length over which the sample is drawn through the SQUID gradiometer coils when the magnetic moment is small. A scan length of 6 cm produced satisfactory results, with a reproducible reversible magnetic moment at fields greater than $H_{irr}(T)$. However, it is well known that, as a consequence of the inhomogeneity of the field produced by the superconducting solenoid, measuring the magnetization with such a scan length at fields close too but *below* H_{irr} corresponds to cycling the sample through minor magnetic hysteresis loops. The magnetic moment then results from the superposition of several ill-controlled shielding current loops and can take on a value that is very different from that expected from the ordinary full critical state. It thus proved very difficult to accurately measure the magnetic moment both above *and* below $H_{irr}(T)$; for the present paper, we chose conditions such as to obtain the most reliable results above $H_{irr}(T)$, and to rely on the ac transmittivity measurements to obtain the screening current below $H_{irr}(T)$.

III. RESULTS AND DATA ANALYSIS

A. Reversible magnetization

Figure 1 shows the reversible magnetization for an optimally doped $Bi_2Sr_2CaCu_2O_{8+\delta}$ single crystal ($T_c = 88.8$ K),[38] irradiated with 10^{11} Pb ions cm^{-2}, which corresponds to a matching field $B_\phi = 2$ T. This value of B_ϕ is comparable to that used in previous studies,[13–17] and the reversible magnetization shows all the features discussed there. Recapitulating, at low fields $H_{irr} < H_a \ll B_\phi$, the absolute value of the magnetization $|M_{rev}|$ decreases more or less proportionally to $\ln(1/H_a)$, in agreement with the London model which has $M_{rev} \approx -(\varepsilon_0/2\Phi_0)\ln(\eta B_{c2}/eB) \equiv M_{rev}^0$.   Here $\varepsilon_0 = \Phi_0^2/4\pi\mu_0\lambda^2(T)$, $\lambda(T)$ is the penetration depth, B_{c2} is the upper critical field, $\mu_0 = 4\pi \times 10^{-7}$ H m^{-1}, $\eta \sim 1$, and $e = 2.718\ldots$. Throughout, the small magnitude of M_{rev} allows us to take $B \approx \mu_0 H_a$. The logarithmic decrease of $|M_{rev}|$ terminates at the field labeled H_{int}, whence $|M_{rev}|$ increases. When $B \gtrsim B_\phi$, $|M_{rev}|$ decreases once again proportionally to $\ln(1/B)$, although the slope $\partial M_{rev}/\partial\ln B$ is markedly higher than the slope at low fields. The logarithmic slopes in either limit are illustrated in Fig. 2, which shows $\partial M_{rev}/\partial\ln B$ as a function of temperature for the same crystal: for fields $B \ll B_\phi$ the logarithmic slope lies markedly below that measured for $B > B_\phi$; also, it goes to zero at a temperature T_1^* that is lower than the temperature T_2^* at which $\partial M_{rev}(B > B_\phi)/\partial B$ goes to zero. Both T_2^* and $\partial M_{rev}(B > B_\phi)/\partial B$ are very similar to the corresponding values measured in the unirradiated crystal.[15] In both cases, unirradiated crystals and irradiated crystals in the high-field limit, one can use the London model[39,40] to extract the value of the penetration depth from $\partial^2 M_{rev}(B > B_\phi)/\partial T \partial\ln B = -\varepsilon_0(0)/2\Phi_0 T_c$, an exercise which yields $\lambda(0) = 180 \pm 30$ nm. The corresponding value of the London penetration
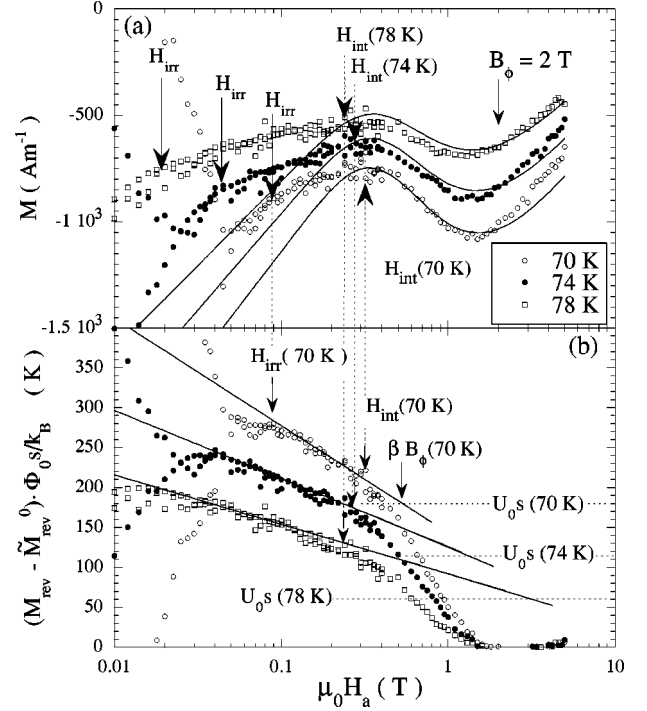

FIG. 1. (a) The reversible magnetization of a heavy-ion-irradiated optimally doped $Bi_2Sr_2CaCu_2O_{8+\delta}$ single crystal ($B_\phi = 2$ T, $T_c = 88.8$ K), for temperatures $T = 70$, 74, and 78 K. The drawn lines represent fits to Eq. (2) with parameter values $\lambda_L(0) = 240$ nm [$\lambda(0) = 180$ nm], $\partial B_{c2}/\partial T = -1.05$ T/K, and $U_0 s \sim 1.5\tilde{\varepsilon}_0 s \approx 1300(1 - T/T_c)$ K. Arrows indicate the field below which the ac transmittivity has a nonzero third harmonic (H_{irr}) and the interaction field H_{int} above which vortex interactions influence the vortex arrangement. (b) ($\Phi_0 s/k_B = 0.23$ K m/A) times the difference between the measured magnetization and the theoretical magnetization in the absence of columnar defect pinning, $\tilde{M}_{rev}^0$ [corrected for the reduction in superfluid density expressed by $\tilde{\lambda}^{-2}(T) = (1 - 2\pi c_0^2 n_d)\lambda^{-2}$]. In the limit $B \ll B_\phi$, the plotted data correspond exactly to the sum of pinning energy and entropy per pancake vortex. Horizontal dotted lines correspond to the *bare* pinning energy $U_0 s = U_0(0)s(1 - T/T_c)^2$, with $\tilde{U}_0(0)s = 4000$ K. This corresponds to the parameter value obtained in Ref. 18, corrected for the change $\lambda \to \tilde{\lambda}$. The drawn lines show the logarithmic extrapolation of the low-field data which permit the determination of the length L_a over which pancakes belonging the same vortex line are aligned on the same column and the factor β describing the fraction of available columns (see Sec. III A 3). For $T = 70$ K, the low-field data obey $U_0 s + T\ln(\beta B_\phi/B)$—i.e., the typical stack length L_a is close to the interlayer spacing; for larger temperatures the prefactor to the logarithm is, unexpectedly, somewhat less. The interaction field H_{int} of (a) is determined as that where the data first deviate from a logarithmic H_a dependence.

depth $\lambda_L(0) \approx 1.35\lambda(0) \approx 240$ nm is in good agreement with literature values for optimally doped $Bi_2Sr_2CaCu_2O_{8+\delta}$.[41] The error [of less than 20% (Ref. 42)] arises because of two reasons. First, the presence of the normal cores of the columnar defects decreases the supercurrent density around each vortex and the strength of intervortex repulsion. This effect can be taken into account by a ''renormalized'' value $\tilde{\lambda}^{-2}(T) = (1 - 2\pi c_0^2 n_d)\lambda^{-2}$ and corresponding $\tilde{\varepsilon}_0 = \Phi_0^2/4\pi\mu_0\tilde{\lambda}^2$ and $\tilde{M}_{rev}^0 = \tilde{\varepsilon}_0/2\Phi_0\ln(\eta B_{c2}/eB)$.[14] More im-
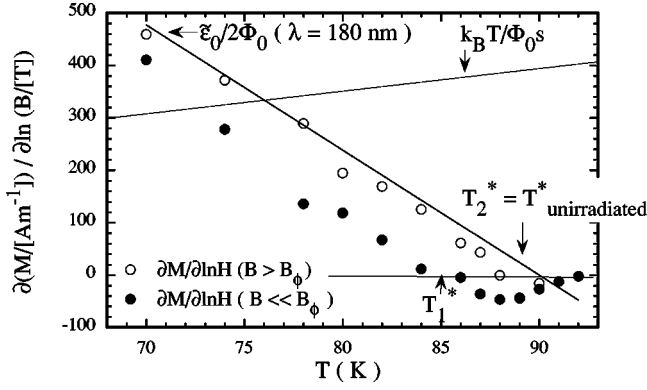
FIG. 2. Logarithmic slopes $\partial M_{rev}/\partial \ln B$ for the same crystal as in Fig. 1, determined in the limits $B > B_\phi = 2$ T and $B \ll B_\phi$, respectively. The drawn lines indicate the magnitude of the theoretical entropy contribution in the 2D limit, $k_B T/\Phi_0 s$, and the prediction of the London model, $M_{rev}^0 = \tilde{\varepsilon}_0/2\Phi_0$.

portant, the presence of thermal fluctuations was predicted to lead to a substantial entropy contribution to the free energy, reflected by an extra term:[43]

$$\frac{\partial^2 M_{rev}}{\partial T \partial \ln B} = \frac{\partial^2 M_{rev}^0}{\partial T \partial \ln B} - \frac{k_B}{\Phi_0 s}. \quad (1)$$

Here, $s \approx 1.5$ nm is half the c-axis parameter of the $Bi_2Sr_2CaCu_2O_{8+\delta}$ material (i.e., the distance between CuO_2 bilayers). From the value $k_B/\Phi_0 s = 4.4$ A m^{-1} K^{-1}, we see that the (constant) contribution of the entropy term[43] can amount to 20% of the temperature derivative of $\partial M_{rev}/\partial \ln B$, at most.

The nonmonotonic field dependence of the reversible magnetization has a straightforward explanation in terms of the lowering of the vortex free energy by pinning onto the columnar defects.[15,17] The magnetization $M_{rev} = -\partial G/\partial B = -\Phi_0^{-1}\partial G/\partial n_v \equiv -\Phi_0^{-1}\mu$, with n_v the vortex density, corresponds to the vortex chemical potential μ and therefore directly measures the energy needed to add a vortex to the system when the field is increased. At low fields many columnar defects are available, so that each and every new vortex can gain a maximum energy per unit length U_0 by becoming trapped in the defect potential; correspondingly $M_{rev} \sim \tilde{M}_{rev}^0 + U_0/\Phi_0$. The pinning of a vortex on an insulating columnar defect entails the redistribution of the super-current towards the vortex periphery, lower maximum current on the vortex core boundary, and a smaller intervortex repulsion. More vortices can therefore enter the sample at fixed magnetic field; hence the absolute value of the magnetization is smaller. However, it is still expected that $M_{rev} \propto \ln(1/B)$ in this regime.[14,15,44] At high fields $\mu_0 H_a > B_\phi$ nearly all columns are occupied, new vortices cannot be trapped on a defect, and hence $M_{rev} \approx \tilde{M}_{rev}^0$, close to the magnetization of an unirradiated sample in the London regime.[15] In the intermediate-field region, $\mu_0 H_{int} < \mu_0 H_a < B_\phi$ in Fig. 1(a), new vortices can become either trapped or free. The proportion of trapped vortices decreases as field increases, leading to the increase of $|M_{rev}|$.

1. Role of intervortex repulsion

The magnetization in the intermediate regime has been estimated in Ref. 14 by considering that the gain in pinning energy for occupation of a particular column should be larger than the loss in energy due to intervortex repulsion when a vortex is moved from its lattice site to the columnar track; assuming a Poisson distribution of distances between tracks, this gives

$$M_{rev} \approx \tilde{M}_{rev}^0 - U_0 \left[1 - \left(1 + \frac{U_0}{\tilde{\varepsilon}_0} \frac{B_\phi}{B} \right) e^{-(U_0/\tilde{\varepsilon}_0)(B_\phi/B)} \right]. \quad (2)$$

In spite of its simplicity, it is possible to obtain acceptable fits to the experimental data at $H_a \gtrsim H_{int}$ using this expression [see Fig. 1(a) and Ref. 32]. In the figure we have used $\partial B_{c2}/\partial T = -1.05$ T/K (Ref. 18) and $\lambda(0) = 180$ nm as determined above. However, for a faithful fit to the peak structure of $|M_{rev}|$ one should assume $U_0/\tilde{\varepsilon}_0$ to be in excess of unity; for example, at 70 K, $U_0/\tilde{\varepsilon}_0 = 1.5$ in Fig. 1. Such large values of U_0 were also found in Refs. 16 and 32; they are incompatible with the theoretical expectation for electromagnetic pinning of vortices,[32,45,46] $U_0 \approx \tilde{\varepsilon}_0 \ln(c_0/\sqrt{2}\xi)$, since they would imply that the column radius c_0 exceeds the coherence length $\xi = 2.2(1 - T/T_c)^{-1/2}$ nm by a factor of 5–6. In Ref. 18, it was found that pinning of the vortex core dominates over electromagnetic pinning in heavy-ion-irradiated $Bi_2Sr_2CaCu_2O_{8+\delta}$ at all temperatures. Then, $U_0 \approx \varepsilon_0(c_0/2\xi)^2$, yielding $c_0 \approx 2.3\xi(0)$. This value is still somewhat high, which shows that the actual pinning mechanism is more complicated than simple core pinning. However, note that even so the magnetization data at fields $H_a \ll H_{int}$ lie much above the theoretical curve.

We thus find that a description that only takes the decrease of the internal energy due to the localization of the vortices on the columnar defects into account is insufficient to describe the large decrease of the low-field magnetization at large B_ϕ. The fact that the low-field logarithmic slope $\partial M/\partial \ln B$ is much smaller than that predicted by Eq. (2) indicates the presence of an extra contribution to the free energy that has a logarithmic dependence $\sim \ln(1/B)$.

2. Role of entropy

In this section we examine the importance of a possible entropy contribution $-TS$ to the free energy. Such a contribution may arise from vortex positional[40,43,44] and order parameter amplitude fluctuations.[40,47,48] The entropy contribution to the free energy is believed to be important in layered superconductors because of the ''crossing point'' behavior observed in the reversible magnetization at T_1^* and T_2^*.[13,15,49,50] Supposing that a description in terms of the London model is appropriate and, hence, that vortex positional fluctuations give the dominant contribution to S, it was derived in Ref. 43 that the crossing point arises in the unirradiated material when the field dependences of the two terms contributing to M_{rev},

$$M_{rev}^{un} = M_{rev}^0 + \frac{k_B T}{\Phi_0 s} \ln\left(\frac{B_0}{B}\right), \quad (3)$$

with derivative

$$\frac{\partial M_{rev}^{un}}{\partial \ln B} = \frac{\varepsilon_0}{2\Phi_0} - \frac{k_B T}{\Phi_0 s}, \tag{4}$$

cancel at $T^* = T_c/[1 + 2k_B T_c/\varepsilon_0(0)s]$. Here B_0 is a field determined by the elemental phase area;[40,43] the fraction B_0/B corresponds to the total number of possible states ("configurations") per vortex. In two dimensions (2D), $B_0 \approx B_{c2}$.[40] In heavy-ion-irradiated layered superconductors, Eq. (3) should be modified: the full result can be found in Ref. 44, but the limiting forms for M_{rev} are

$$M_{rev} \approx \tilde{M}_{rev}^0 + \frac{U_0}{\Phi_0} + \frac{k_B T}{\Phi_0 s} \ln\left(\frac{B_\phi}{B}\right) \quad (B \ll B_\phi), \tag{5}$$

$$M_{rev} \approx \tilde{M}_{rev}^0 + \frac{k_B T}{\Phi_0 s} \ln\left(\frac{B_0}{B}\right) \quad (B \gg B_\phi, \ U_0 \to 0). \tag{6}$$

These are again valid in the 2D limit where the positions of pancake vortices in neighboring layers are uncorrelated. The logarithmic field dependence of the second term of Eq. (5) now depends on the number ($\sim B_\phi/B$) of columnar defect sites available to each pancake vortex.

In order to estimate the importance of the entropy contribution to the experimentally measured magnetization, we return to the temperature dependence of the logarithmic slopes $\partial M_{rev}/\partial \ln B$ in Fig. 2. Note that, according to Eqs. (3)–(6), $\partial M_{rev}/\partial \ln B$ is equal to the difference between two large terms:

$$\frac{\partial M_{rev}}{\partial \ln B} = \frac{\partial \tilde{M}_{rev}^0}{\partial \ln B} - \frac{k_B T}{\Phi_0 s}. \tag{7}$$

However, these terms have very different temperature derivatives, equal to $-\tilde{\varepsilon}_0(0)/2\Phi_0 T_c$ and $-k_B/\Phi_0 s$, respectively. The ratio between the temperature derivatives is equal to $2Gi^{1/2}$, where Gi is the 2D Ginzburg number that determines the regime of reduced temperature $t(T) = (T_c - T)/T_c$ over which the entropy contribution to the free energy is dominant. For optimally doped $Bi_2Sr_2CaCu_2O_{8+\delta}$, $2k_B T_c/\varepsilon_0(0)s \approx 0.19$, i.e., $Gi \approx 0.01$; for our overdoped material, $Gi \approx 0.003$. The value 0.19 means that the error in the $\tilde{\lambda}(0)$ value deduced from the reversible magnetization, arising from an entropy contribution to the free energy, cannot exceed 19% (11% for the overdoped crystals). Inserting the experimental $\tilde{\lambda}$ value back into $\tilde{M}_{rev}^0$, and comparing the result to the full measured magnetization, we find that for $B \gg B_\phi$ as well as for unirradiated crystals,[49] the entropy contribution to $\partial M_{rev}/\partial \ln B$ does not exceed $0.1 \, k_B T/\Phi_0 s$ (see Fig. 2). This excludes an interpretation of the crossing point in terms of quasi-2D vortex positional fluctuations only: for example, Eq. (3) would lead to $T^* = 75$ K. More generally, vortex translational degrees of freedom do not lead to a major modification of the magnetization of unirradiated crystals (or irradiated crystals at fields above B_ϕ) in the London regime. The entropy contribution to the free energy only starts to be important in the critical fluctuation regime.

With respect to this, we note that the analysis of Ref. 49 has demonstrated that the crossing point in unirradiated $Bi_2Sr_2CaCu_2O_{8+\delta}$ crystals indeed lies in the regime of (2D)

critical fluctuations. An adequate description, valid for $B > \frac{1}{3}t(\partial B_{c2}/\partial t)_{T=T_c}$, was obtained in Ref. 48 by expanding the order parameter in terms of lowest Landau level (LLL) eigenfunctions. The expression for M_{rev} derived in Ref. 48 [which also predicts $\partial M_{rev}/\partial \ln B \to \varepsilon_0/2\Phi_0$ for $t \gg t(T^*)$] well describes the experimental data for both unirradiated $Bi_2Sr_2CaCu_2O_{8+\delta}$ (Ref. 48) and irradiated $Bi_2Sr_2CaCu_2O_{8+\delta}$ above the matching field.[15] In Fig. 2, the $B \gg B_\phi$ data lie outside the London limit for $T \gtrsim 80$ K, and within the LLL regime for $T \gtrsim 84$ K. An interpretation of the field-independent magnetization at T_2^* in terms of vortex positional fluctuations (order parameter phase fluctuations) only is thus inappropriate.

The situation is totally different for $B \ll B_\phi$, at which one has a significantly larger value $TS \gtrsim 0.3 k_B T/\Phi_0 s$. This means that the introduction of many extra possible (columnar defect) sites within a vortex lattice unit cell leads to a large (configurational) entropy contribution. Moreover, a description in terms of the London model will turn out to be adequate in this field regime.

3. Interlayer coupling: Dependence on matching field

The small entropy contribution to the reversible magnetization for $B \gtrsim B_\phi$ suggests that even in the vortex liquid, significant positional correlations remain between vortex pancakes in adjacent layers. In that case, S is reduced with respect to its value in the 2D limit: the alignment of pancakes in different layers means that the relevant entities are stacks (of length L_a) comprising several pancakes. The entropy contribution in the regime $B \ll B_\phi$ where all pancakes are trapped by a column can be estimated as $TS = k_B T \ln W = k_B T \ln N_c^{L_s/L_a}$, with $N_c \equiv \beta B_\phi/B$ the number of columns available to each stack of pancakes, L_s the length of the sample in the field direction, and L_a the length $\|c$ over which the pancakes are aligned on the same columnar track. The number $1 - \beta$ is the fraction of columns that is inaccessible due to intervortex repulsion. In the quasi-2D limit, $L_a = s$, but in general L_a can be estimated from the balance between elastic energy and thermal energy: $\tilde{\varepsilon}_1 \Phi_0/B_\phi L_a \sim k_B T$ ($\tilde{\varepsilon}_1 \approx \tilde{\varepsilon}_0/\gamma^2$ is the line tension and γ the anisotropy parameter). Hence the entropy contribution per unit length $TS = k_B T \ln N_c^{L_s n_d k_B T/\tilde{\varepsilon}_1}$ and the magnetization[51]

$$M_{rev} = M_{rev}^0 + \frac{U_0}{\Phi_0} + \frac{k_B T}{\Phi_0 s}\left(\frac{k_B T}{\tilde{\varepsilon}_0 s}\right)\frac{B_\phi}{B_{cr}} \ln\left(\frac{\beta B_\phi}{B}\right) \tag{8}$$

$$= M_{rev}^0 + \frac{U_0}{\Phi_0} + \frac{k_B T}{\Phi_0 s}\frac{s}{L_a} \ln\left(\frac{\beta B_\phi}{B}\right) \quad (B_\phi < B_{cr}\tilde{\varepsilon}_0 s/k_B T). \tag{9}$$

The crossover field $B_{cr} \equiv \Phi_0/(\gamma s)^2$ delimits the (low-field) regime where tilt deformations of the vortex lattice with wave vector $\sim 4\pi(B/\Phi_0)^{1/2}$ are more difficult to excite than shear deformations with a similar wave vector, from the high-field regime where the inverse is true. The contribution TS adds a supplementary logarithmic dependence on B at low fields, in agreement with the difference between the experimental $\partial M_{rev}/\partial \ln B$ observed at $B \ll B_\phi$ and $B > B_\phi$, respectively [see Fig. 1(a)].
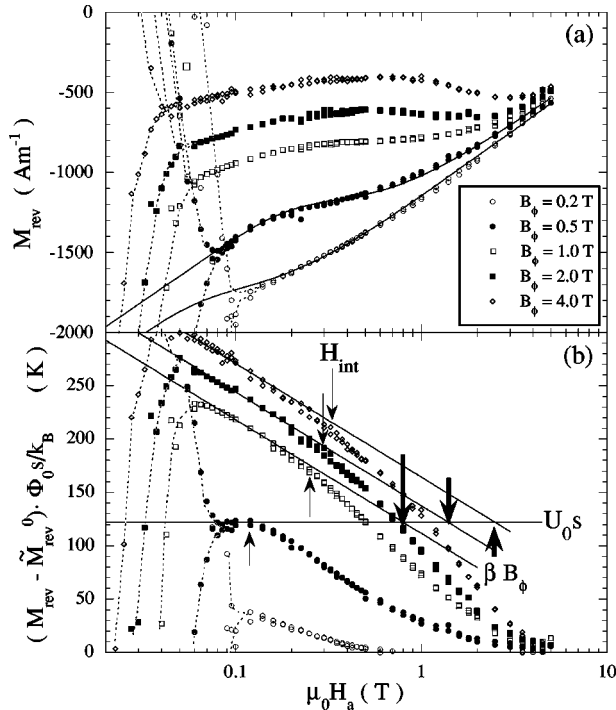
FIG. 3. (a) Reversible magnetization of lightly overdoped $Bi_2Sr_2CaCu_2O_{8+\delta}$ at $T/T_c = 0.89$, for matching fields 0.2 T$< B_\phi$ <4 T. The critical temperature $T_c \approx 83.1$ K, except for $B_\phi = 2$ T ($T_c = 81$ K) and $B_\phi = 4$ T ($T_c = 78.7$ K). The drawn lines through the data points for $B_\phi = 0.2$ and 0.5 T represent fits to Eq. (2) with parameter values $\lambda(0) = 140$ nm and $U_0 s = 120$ K; dotted lines are guides to the eye, representing the magnetization in the irreversible regime. (b) $\Phi_0 s / k_B$ times the difference between the measured magnetization and the theoretical magnetization in the absence of columnar defect pinning, $\tilde{M}_{rev}^0$ [corrected for the reduction in superfluid density expressed by $\tilde{\lambda}^{-2}(T) = (1 - 2\pi c_0^2 n_d)\lambda^{-2}$]. In the limit $B \ll B_\phi$, the plotted data correspond exactly to the sum of pinning energy and entropy per pancake vortex. The drawn lines show the *bare* pinning energy per pancake vortex $U_0 s$ (corresponding to the low-field limit of the $B_\phi = 0.5$ T data), and, for $B_\phi \gtrsim 1.0$ T, $U_0 s$ plus the configurational entropy contribution TS $\approx (k_B T / \Phi_0 s) \ln(\beta B_\phi / B)$ arising from the possibility of individual pancake vortices to occupy different column sites. The fraction β $\approx 1/2$ can be extracted from the intercept with the horizontal $U_0 s$ line, and is indicated by the bold arrows. The fields H_{int} where intervortex interactions begin to influence the magnetization can be determined as the field of first deviation from a logarithmic field dependence and are indicated using the thin arrows. Dotted lines are guides to the eye, indicating data in the irreversible regime.

In Ref. 13, it was claimed that the maximum in $|M_{rev}|$ can be nearly entirely explained by the reduction in TS, caused by pancake alignment (''recoupling'') and the concomitant decrease in s/L_a. This claim can be tested by using Eq. (9), which permits a direct estimate of the correlation length L_a. Starting from the values of $\partial M_{rev}/\partial \ln B$ determined above, one would have $L_a \lesssim s/0.3 \approx 3s$ for $\mu_0 H_a$ $\ll B_\phi = 2$ T and $L_a \gtrsim 10s$ for $\mu_0 H_a \gtrsim B_\phi$, similar to the value $L_a \approx 15s$ recently obtained by Morozov *et al.*[27] and in qualitative agreement with the assumption of Ref. 13.

A more stringent approach is to consider the dependence of M_{rev} on matching field, i.e., the dependence on the number of available states. Figure 3(a) shows the magnetization
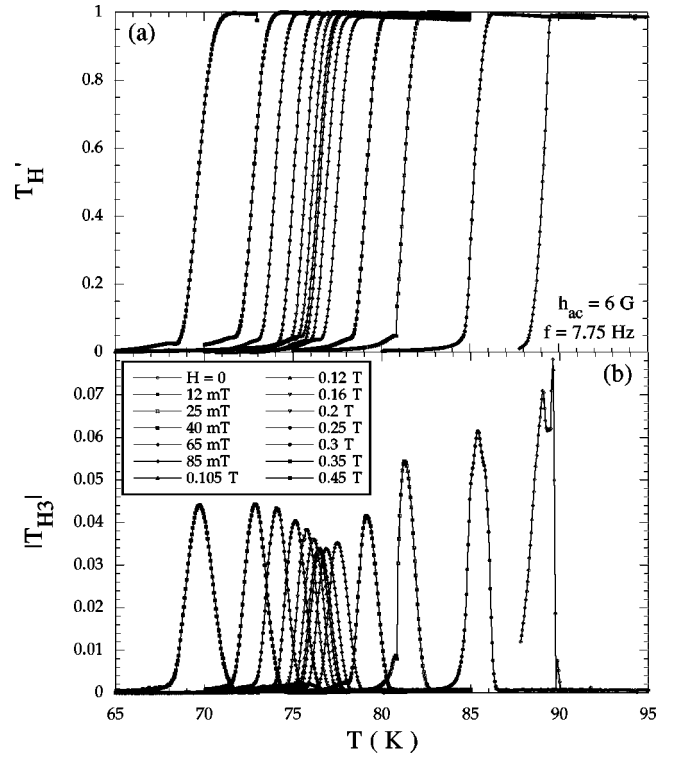

FIG. 4. In-phase fundamental transmittivity T_H' (a) and third-harmonic amplitude $|T_{H3}|$ (b) measured on an optimally doped $Bi_2Sr_2CaCu_2O_{8+\delta}$ single crystal ($T_c = 90.0$ K), irradiated with 5.8 GeV Pb ions to a matching field $B_\phi = 0.5$ T. The measurement frequency was 7.753 Hz and the ac field amplitude $h_{ac} = 6$ Oe. dc field values are as indicated.

of a series of lightly overdoped $Bi_2Sr_2CaCu_2O_{8+\delta}$ crystals [$T_c \approx 83$ K, $\lambda(0) \approx 140$ nm], irradiated to different ion fluences corresponding to matching fields ranging between 0.2 T and 4.0 T. The figure shows that there is a large dependence of the low-field magnetization on the density of columns, which irrevocably indicates the importance of the configurational entropy contribution to M_{rev} in that regime. Namely, if S were zero, the low-field limits of M_{rev} would have been equal to $M_{rev}^0 + U_0/\Phi_0$, independent of B_ϕ [see Eqs. (2) and (5)]. Furthermore, the data at $B_\phi \gtrsim 1$ T confirm the extra logarithmic field dependence (8) for $B \ll B_\phi$. For the crystal with $B_\phi = 0.5$ T, the low- and high-field limits of $\partial M_{rev}/\partial \ln B$ are nearly equal, implying that at this temperature, the entropy contribution to $\partial M_{rev}/\partial \ln B$ lies within the error bar of $0.1 k_B T/\Phi_0 s$ found in Sec. III A 2 (see also Ref. 17, Fig. 3). Hence, for this matching field and temperature, it follows from Eq. (9) that pancakes are aligned into stacks of length $L_a \gtrsim 10s$ over the entire considered field range. It means that for low matching fields it is allowed to ignore the entropy contribution. One can then confidently determine $U_0 s$ from the difference between the measured magnetization and the low-field limit of $\tilde{M}_{rev}^0$.[18,53] Inserting the obtained value $U_0 s \approx 120$ K (for $\tilde{\varepsilon}_0 s \approx 160$ K at 74 K) back into Eq. (2) yields good fits to the data for $B_\phi = 0.2$ and 0.5 T, as shown by the drawn lines in Fig. 3. Such fits are not possible at higher B_ϕ due to the increasing importance of the entropy contribution, which, even at $B_\phi = 1$ T, already accounts for half the change of the low-field reversible magnetization

with respect to that of an unirradiated crystal. The determination of a ''pinning energy'' from the difference between the low-field data and the extrapolation to low fields of the data for $B \gg B_\phi$ can then introduce an error of more than a factor of 2.

The parameters L_a and β can, in principle, be directly evaluated by subtracting $\tilde{M}_{rev}^0$ from the measured magnetization. This procedure yields a quantity that at low fields is rigorously equal to the sum of the pinning energy per pancake vortex and temperature times entropy [Fig. 3(b)]. The low-field limit of the $B_\phi = 0.5$ T data corresponds to the bare pinning energy $U_0 s$—this value is indicated by the horizontal line in Fig. 3(b). The results for the crystals with $B_\phi \geq 1$ T exceed $U_0 s$ at $B \ll B_\phi$ because of the entropy contribution to the free energy. From the logarithmic field derivative and the extrapolation to $U_0 s$ we find that, at $T/T_c = 0.89$, $L_a(B \ll B_\phi) \approx s$ and $\beta \approx \frac{1}{2}$, independent of B_ϕ. Thus, the magnetization at low fields and $B_\phi \geq 1$ T is well described by

$$M_{rev} = \tilde{M}_{rev}^0 + \frac{U_0}{\Phi_0} + \frac{k_B T}{\Phi_0 s} \ln\left(\frac{B_\phi}{2B}\right), \quad (10)$$

as illustrated by the drawn lines through data in Fig. 3(b). The first deviation of the experimental data from these lines as the field is increased, at the ''interaction field'' H_{int}, indicates that both configurational entropy and the total pinning energy start to decrease due to the effect of vortex interactions. Entropy decreases because of the limitation of accessible column sites, which is the consequence of intraplane pancake repulsion; it can be expressed by a diminishing β; the translational invariance of the system along the column direction and the attractive interaction between pancakes in adjacent layers will then lead to pancake vortex alignment and the supplementary decrease of S through the increase of L_a. The *total* pinning energy U_p can only go down appreciably if free (or ''interstitial'') vortices, not trapped on a columnar track, start to appear, again as a result of intraplane pancake repulsion which prohibits certain vortices from finding a favorable column site. From Fig. 3, it is seen that near H_{int}, the pinning energy (obtained from the $B_\phi = 0.5$ T data) and the entropy contribution to the free energy are comparable in magnitude when $B_\phi \geq 1$ T; hence *both* contributions should always be taken into account when describing the shape of the $M_{rev}(B)$ curve.

We have attempted to carry out the same analysis for constant matching fields $B_\phi = 0.5$, 1, and 2 T, and different T [see Fig. 1(b) for $B_\phi = 2$ T]. In this case, the problem arises that the bare pinning energy cannot easily be established. It was therefore chosen to take the result of Ref. 18 (where $B_\phi = 0.5$ T), $U_0(T) = U_0(0)(1 - T/T_c)^2$ for core pinning, and to correct the value $U_0(0) = 4300$ K obtained there for the larger density of columns in those cases where $B_\phi > 0.5$ T. The difference between the low-field data and these values, represented by dashed lines in the Fig. 1(b), again corresponds to temperature times the configurational entropy. For $B_\phi = 1$ and 2 T, it is found that $TS(B = \beta B_\phi/e) \approx T$, indicating that $L_a \approx s$. The logarithmic field dependence at $T = 74$ and 78 K, as well as the magnitude of the logarithmic slopes, also agrees with $L_a/s \approx 1-2$. However, since the logarithmic slopes should, in the representation of Fig. 1(b), be equal to T, the predicted temperature dependence is not
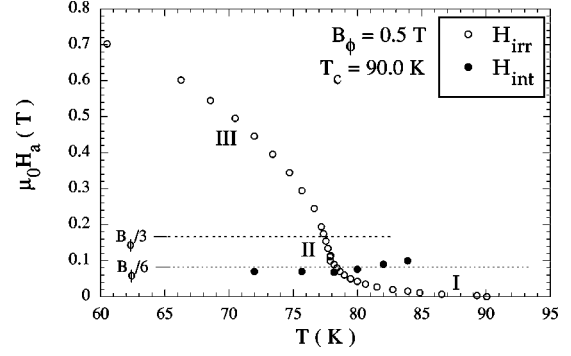

FIG. 5. Irreversibility field $H_{irr}(T)$, at which a third harmonic ac response $|T_{H3}|$ can first be measured upon cooling the crystal (the same as in Fig. 4) in a magnetic field ($\bigcirc$). The roman numerals indicate the field regimes described in the text. Also indicated are the fields $H_{int}(T)$ determined from reversible magnetization measurements on the same crystal ($\bullet$).

well obeyed. In fact, for the data at $T = 70$ K it is difficult to identify any substantial field range over which $TS \propto \ln(1/B)$. This is in contrast to data for $B_\phi = 0.5$ T where a low-field logarithmic dependence can be identified at all investigated temperatures.[17,18] Hence, accurate values for H_{int} can be determined only for small B_ϕ (see Fig. 5 for $B_\phi = 0.5$ T). At low B_ϕ, the entropy contribution to the free energy is unimportant. The interaction field then delimits the low-field regime where vortices are pinned independently on the columnar tracks, from the high-field regime where intervortex repulsion entails the presence of unpinned (''free'' or ''interstitial'') vortices. Results for larger matching field can only be obtained in a restricted temperature range $T_{irr} < T < T_c(1 - Gi)$ (see Fig. 6 for $B_\phi = 1$ T). Here, the interaction field separates the regime of individual vortex pinning from high fields at which the intervortex repulsion determines the optimum pinned configuration but does not necessarily lead to the presence of ''free'' vortices.
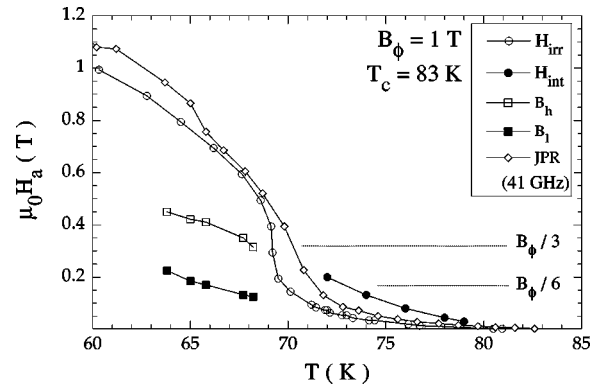

FIG. 6. Irreversibility field $H_{irr}(T)$ determined for lightly overdoped $Bi_2Sr_2CaCu_2O_{8+\delta}$ (Ref. 56) with $B_\phi = 1$ T ($\bigcirc$). The crystal was chosen so as to have $T_c = 83.1$ K comparable to the sample used to obtain the JPR peak data of Ref. 11 [also shown ($\Diamond$)], as well as to the crystal of Ref. 26. The characteristic fields B_l ($\blacksquare$) at which the c-axis conductivity starts to increase and B_h ($\square$) at which it starts its final decrease (Ref. 26) are displayed as solid and open squares, respectively. The interaction fields $H_{int}(T)$ determined from reversible magnetization measurements are drawn as solid circles ($\bullet$).

We note that, in the analysis presented in Fig. 1(b), the assumption of $U_0 s \approx \varepsilon_0(0)s(1 - T/T_c)$ for electromagnetic pinning of vortices yields the rather unlikely result that the entropy contribution to the free energy rapidly *decreases* as function of temperature.

B. Relation with the phase diagram

In order to correlate the vortex arrangement on the columnar tracks as revealed by the reversible magnetization measurements with the phase diagram, we have performed measurements of the ac transmittivity as described in Sec. II B. Typical results for the in-phase fundamental and third harmonic amplitude are shown in Fig. 4 for optimally doped $Bi_2Sr_2CaCu_2O_{8+\delta}$ ($T_c = 90.0$ K) with $B_\phi = 0.5$ T.[54] The corresponding fields $H_{irr}(T)$ at which a third harmonic response is first detected are plotted in Fig. 5. Note that due to the different effective measurement frequencies, $f = 7.753$ Hz in the ac shielding experiment versus $f \sim 10^{-2}$ Hz for magnetization measurements using the SQUID, the H_{irr} values plotted in the figure lie much above the apparent H_{irr} values extracted from the closing of the magnetic hysteresis loops or merger of zero-field-cooled and field-cooled data obtained with a SQUID magnetometer.[8,11–13] The same is indicated in Fig. 1(a), which shows the position of H_{irr} determined from transmittivity measurements on the magnetization curve. The magnetization data show a break at H_{irr}, reflecting the inadequacy of moving sample SQUID magnetometry for measurements in the regime $H_a \lesssim H_{irr}$. Another reason for the much lower $H_{irr}(T)$ values of Refs. 12 and 13 is the fact that those authors used lightly underdoped crystals. While T_c can be similar for underdoped and overdoped samples, it was recently shown that the irreversibility lines for the irradiated material vary widely as a function of oxygen content.[55]

The irreversibility field displays three distinct regimes as a function of temperature. Upon lowering the temperature from T_c, $H_{irr}(T)$ first increases exponentially (I);[3,6,8,36] at $T \simeq 77$ K, H_{irr} increases sharply (II), before bending over to an approximately linear temperature dependence below 70 K (III). The same behavior is found for other matching fields; see, e.g., Fig. 6 for $B_\phi = 1$ T. For comparison, the same figure shows characteristic fields extracted from c-axis conductivity and JPR measurements. It is seen that the different regimes of the irreversibility line $H_{irr}(T)$ are faithfully reproduced by the position of the JPR peak;[11] for a suitably chosen measurement frequency (here, 41 GHz) the two lines lie very close together, suggesting that the onset of linear vortex diffusion (and, hence, the disappearance of long-range ab-plane phase coherence) indicated by $H_{irr}(T)$ is intimately related to the drop in c-axis phase coherence expressed by the JPR peak.

Also plotted in either figure are the H_{int} data for the same crystals. For the optimally doped crystal ($B_\phi = 0.5$ T) of Fig. 5, it was possible to obtain H_{int} values directly from the reversible magnetization for fields *below* the irreversibility field by exploiting the torque data of Ref. 17. The reversible magnetization curves in this case were measured with the magnetic field applied at a substantial angle with respect to the c axis and the column direction. It was shown previously that in such a configuration, the reversible magnetization depends only on the field component H_z parallel to the c axis;
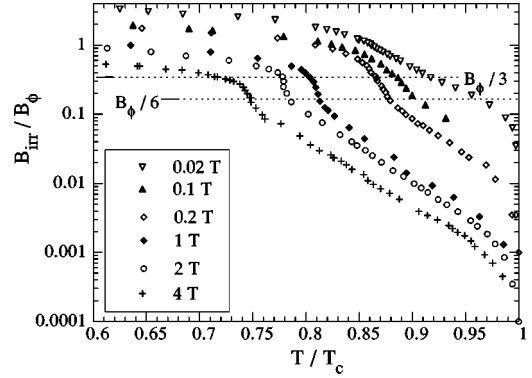

FIG. 7. Dependence of $H_{irr}(T)$ on matching field. Displayed are the values $\mu_0 H_{irr}(T)/B_\phi$ for a series of crystals grown at the University of Tokyo, irradiated with 5.8 GeV Pb ions to matching fields between 0.02 T and 4 T; data are plotted as a function of T/T_c, where T_c is the value *after* irradiation (e.g., $T_c = 86.2$ K for $B_\phi = 2$ T).

within experimental error, the magnetization curve $M_{rev}(H_z)$ is the same regardless of the direction of the total magnetic field. Simultaneously, applying the field at an angle lowers the irreversibility field H_{irr} to a much lower value than when the field is aligned with the columnar defects.[6]

It appears that the field H_{int} intercepts the irreversibility line exactly at the point $\mu_0 H_a \approx \frac{1}{6} B_\phi$ where H_{irr} starts its steep rise (Fig. 5). This strongly suggests that the reduction of vortex mobility causing the increase in $H_{irr}(T)$ is the consequence of intraplane vortex repulsion and the reduction of the number of sites available to a given vortex. The H_{int} data nicely coincide with the recoupling field obtained in Refs. 11 and 12. For $B_\phi = 1$ and 2 T, reliable H_{int} data could not be obtained in the temperature interval spanning the irreversibility line. The data in Fig. 6 show that for temperatures well in excess of H_{irr}, H_{int} decreases with increasing T. The temperature dependence of the interaction field, reminiscent of that of the high-field part of the irreversibility line, seems to extrapolate to the field B_h where the c-axis conductivity starts its ultimate decrease.[26] Note that H_{int} never increases beyond the field $\mu_0 H_a \approx \frac{1}{6} B_\phi$ at which the recoupling transition is expected. This particular fraction of the matching field, $\frac{1}{6} B_\phi$, seems to be quite robust. Figure 7, which displays the evolution of $H_{irr}(T)$ with B_ϕ, shows that for 0.1 T $\leqslant B_\phi \leqslant 4$ T the steep rise of the irreversibility line always starts near $\mu_0 H_a \approx \frac{1}{6} B_\phi$. This is in contradiction to numerical work[57] and previous magnetization studies[13] which reported significant features in the phase diagram at $\mu_0 H_a \approx \frac{1}{3} B_\phi$. Figure 7 shows that, whereas for the values of the matching field $B_\phi = 1$ and 2 T, most commonly investigated in the literature,[11–13,57] the fraction $B_\phi/3$ coincides with the crossover from regime (II) to regime (III) in $H_{irr}(T)$, this is by no means true for other values of B_ϕ. The results also show that the reported scaling of the irreversibility line with B_ϕ reported in Ref. 3 is by no means to be taken strictly.

IV. DISCUSSION

A number of significant results emerge from the above. The most notable is that the introduction of amorphous co-

lumnar defects into the matrix of the layered superconductor decreases the free energy in the London regime not only through vortex pinning, but also through an additional configurational entropy, which appears when a sufficiently large number of extra sites become available to the pancake vortices. This extra contribution can be comparable to or larger than the pinning energy. Previously presented values of the pinning energy extracted from the reversible magnetization of crystals with relatively high matching fields[14–16,32] should thus be considered with reserve. More accurate measurements of the pinning energy for crystals with lower B_ϕ were recently presented in Ref. 18. The pinning energies obtained in this paper are in agreement with those of Ref. 18 and with the vortex-core pinning model, $U_0 \approx \varepsilon_0(c_0/2\xi)^2$.[21] This means that even in the vortex liquid state, vortices are, certainly in the regime $B \ll B_\phi$, strongly bound to the columnar defects. Thermally induced vortex wandering from the tracks would have resulted in a pinning energy contribution U_0/Φ_0 that is exponentially small with respect to the total magnetization.[52] The neglect of the entropy contribution also accounts for the discrepancy between experimental results and the numerical simulations of Ref. 31. The curves calculated in Ref. 31 are close to what would be expected in the (near) absence of an entropy contribution (see, for example, data at $B_\phi = 0.2$ T). Conversely, the use of Eq. (5) overestimates the entropy contribution in many cases and yields pinning energies that are manifestly too small.[44]

The measurement of the reversible magnetization as a function of column density allows a direct determination of the extra entropic contribution TS (Fig. 3), and its dependence on field and temperature. The mechanisms by which the free energy is lowered becomes apparent if one considers the rather peculiar dependence of TS on the density of sites at constant field, illustrated in Fig. 8. At low B_ϕ, TS remains small in comparison with other terms contributing to the free energy. This can also be inferred directly from the near equality of the low- and high-field limits of the logarithmic slope of the reversible magnetization for $B_\phi \lesssim 0.5$ T.[17,18] At high matching field, TS follows a logarithmic dependence on ion dose. We interpret this behavior as follows. At low irradiation doses, the increase in entropy with increasing columnar defect density arises from the dissociation of vortex lines into shorter and shorter stacks of length L_a localized on different columns; the entropic part of the free energy (in the vortex liquid phase) then obeys Eq. (8), with $\beta \sim \frac{1}{2}$. As a result, TS increases as $B_\phi \ln B_\phi$, which explains its rapid rise between $B_\phi = 0.5$ T and 1 T and the quite important change in the low-field magnetization between these matching fields. Once the length of a typical stack has decreased to a single pancake vortex, this mechanism can no longer be operative. The entropy now increases as $\ln B_\phi$, corresponding to the possibility for each single pancake to occupy different columnar defects. The evolution of the entropy with increasing matching field can be described by the optimization of the total free energy gain, obtained from the balance between the entropy gain and the loss in intervortex interaction energy. At small B_ϕ, there are few near-lying columnar defect sites per vortex line—the access to far-lying sites is prohibited by intervortex repulsion. Hence, vortices are on average well aligned on the same site. For increasing B_ϕ, more and more near-lying defect sites become available, and the free energy
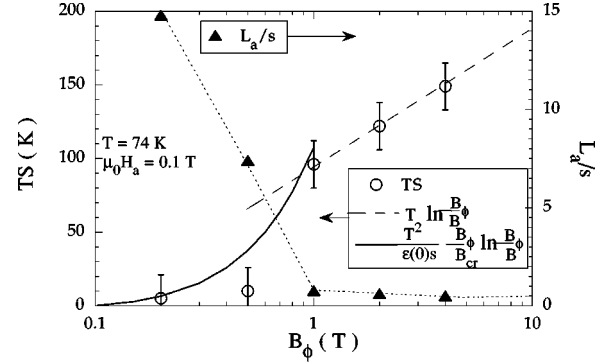

FIG. 8. Entropy contribution to the free energy of heavy-ion-irradiated lightly overdoped $Bi_2Sr_2CaCu_2O_{8+\delta}$ ($T_c = 83$ K) as a function of matching field ($\bigcirc$), for $T = 74$ K and applied field $\mu_0 H_a = 0.1$ T. The entropy rises steeply between $B_\phi = 0.5$ and 1 T, from where it increases logarithmically as a function of B_ϕ. This behavior is in qualitative agreement with the dissociation of individual vortex lines into stacks of length L_a at low defect density (few available sites per vortex), for which the prediction $TS \propto B_\phi \ln B_\phi$ is indicated by the curved solid line; at higher matching fields, the length of the typical stack has decreased to the layer spacing s—the dependence then becomes $TS \propto \ln B_\phi$, corresponding to the configurational entropy associated with the possibility for each pancake vortex to occupy different columns (dashed straight line). The corresponding values of L_a are indicated by the solid triangles (the dotted line is a guide to the eye). The parameter values used are $\varepsilon_0 s = 1500$ K and $B_{cr} = 0.4$ T (Ref. 58), i.e., $\gamma = 55$ (Ref. 59).

can be lowered through the dissociation of vortex lines, first into stacks of pancakes located on adjacent columns and finally into single pancakes wandering between available column sites.

The same explains the field dependence of TS (Figs. 1 and 3). As more and more vortices are added, fewer sites are available per vortex. First, the entropy contribution drops (logarithmically) because fewer defect sites are available to each pancake. At higher fields, pancakes belonging to the same vortex line become aligned on the same site, be this on a columnar defect or on an interstitial site. This leads to a reduction in vortex mobility and to the increase of the c-axis critical current measured by JPR (Refs. 12 and 30) and of the c-axis conductivity.[26,27,60]

It is to be stressed that in the presence of columns the low-field entropy contribution to the free energy is much *larger* than that in unirradiated crystals, at odds with the prediction of Eqs. (3) and (5).[44] A qualitative explanation for this is that, whereas in unirradiated crystals one has one local energy minimum per vortex lattice unit cell, the presence of a columnar defect density $n_d > B/\Phi_0$ amounts to the presence of several energy minima per cell, permitting the ''roughening'' of vortex lines (i.e., their spreading over different columnar defects). Entropy decreases as a function of B until at $B \sim \frac{1}{2}B_\phi$ it attains a value close to that measured in unirradiated samples, corresponding to approximately one site per vortex. From this field onwards, it becomes difficult to obtain a reliable estimate of the alignment length L_a from reversible magnetization. This is because of the ''error bar'' introduced by the large value of the Ginzburg number Gi. We have seen in Sec. III A 2 that there is an uncertainty of

the order $0.1k_BT/\Phi_0 s$ when one determines the relative importance of the different terms contributing to $\partial M_{rev}/\partial \ln B$. In particular, one cannot estimate the entropy contribution to better than $0.1k_BT/\Phi_0 s$, corresponding to a lower bound $L_a \lesssim 10s$. The same holds for unirradiated crystals. Whereas in the irradiated superconductor the dissociation of vortex lines into stacks of pancakes (within a unit cell) certainly lowers interplane correlations of the phase of the superconducting order parameter, it does not necessarily imply the loss of long-range phase coherence. This is likely destroyed near the irreversibility line, as linear activated motion of (pancake) vortices becomes possible.

The questions of pancake vortex alignment, phase coherence, and the recoupling transition reported in Refs. 11–13 are intimately related. From reversible magnetization, we have determined the field H_{int} at which intervortex repulsion determines the vortex pancake arrangement in the presence of columnar defects. This is in very good agreement with the recoupling field obtained in Refs. 11,12, and coincides with the rapid rise of $H_{irr}(T)$. It seems that the same intraplane vortex repulsion responsible for vortex alignment also decreases the vortex mobility, expressed by the peak in the critical current density measured in Refs. 13 and 61, and by the increase in $H_{irr}(T)$ into regime (II) at $\frac{1}{6}B_\phi$. As for the increase in vortex mobility and the decrease of c-axis conductivity at the crossover of H_{irr} from regime (II) to the high-field region (III), it is likely that it corresponds to the field at which the number of free vortices becomes comparable to or exceeds the number of vortices trapped on a columnar defect. This field can be roughly estimated as that at which $U_p + TS$ [Figs. 1(b) and 3(b)] has decreased to half its value at H_{int}. For $B_\phi \gtrsim 1$ T, it amounts to roughly the value $\frac{1}{3}B_\phi$ cited in Ref. 13; for lower matching fields it lies closer to B_ϕ. In all cases, it lies close to the crossover in question. Thus, we identify regime (III) of $H_{irr}(T)$ as that in which the number of free vortices exceeds the number of trapped ones and in which vortex mobility is determined by plastic vortex creep.[21]

V. CONCLUSION

Reversible magnetization measurements have been analyzed in order to determine the relative importance of pinning energy and entropy contributions to the free energy of heavy-ion-irradiated $Bi_2Sr_2CaCu_2O_{8+\delta}$ single crystals. We have found that in unirradiated crystals the entropy contribution to the free energy in the London regime is relatively minor. This is also true in irradiated crystals with small matching fields $B_\phi \lesssim 0.5$ T, but not for irradiated crystals with large $B_\phi \gtrsim 1$ T and fields $B \ll B_\phi$. Then, the configurational entropy contribution to the free energy is greatly enhanced with respect to its value in unirradiated crystals, and can easily exceed the pinning energy of a vortex on a columnar defect by more than a factor of 2. The large entropy contribution at high B_ϕ is a consequence of the dissociation of vortex lines into individual pancake vortices localized on different columnar defect sites. As B/B_ϕ is increased, intervortex repulsion causes the pancakes belonging to the same stack to align onto the same columnar defect. It was possible to obtain a lower bound $L_a \sim 10s$ on the length over which pancakes are aligned at $B \approx B_\phi$. Vortex interactions become important at the field $H_{int} \sim \frac{1}{6}B_\phi$; at this field, which delimits the regime of pinning of individual vortices and which corresponds to the recoupling field measured by Josephson plasma resonance, the irreversibility field sharply increases. Above H_{int}, the repulsive interaction between vortices causes both the vortex mobility to decrease and pancake alignment to increase. At higher fields $\gtrsim \frac{1}{3}B_\phi$, free vortices outnumber those that are trapped on a columnar defect. This causes the decrease of c-axis resistivity and a second crossover of the irreversibility field, to a regime where it is determined by plastic creep.

[1] V. Hardy, J. Provost, D. Groult, M. Hervieu, B. Raveau, S. Durčok, E. Pollert, J. C. Frison, J. P. Chaminade, and M. Pouchard, Physica C **191**, 85 (1992).

[2] M. Koncykowski, Y. Yeshurun, L. Klein, E. R. Yacoby, N. Chikumoto, V. M. Vinokur, and M. V. Feigel'man, J. Alloys Compd. **195**, 407 (1993).

[3] V. Hardy, Ch. Simon, J. Provost, and D. Groult, Physica C **205**, 371 (1993).

[4] L. Klein, E. R. Yacoby, Y. Yeshurun, M. Konczykowski, and K. Kishio, Phys. Rev. B **48**, 3523 (1993).

[5] M. Konczykowski, N. Chikumoto, V. M. Vinokur, and M. V. Feigel'man, Phys. Rev. B **51**, 3957 (1995).

[6] C. J. van der Beek, M. Konczykowski, V. M. Vinokur, T. W. Li, P. H. Kes, and G. W. Crabtree, Phys. Rev. Lett. **74**, 1214 (1995).

[7] D. Zech, S. L. Lee, H. Keller, J. Blatter, B. Janossy, P. H. Kes, and T. W. Li, Phys. Rev. B **52**, 6913 (1995).

[8] D. Zech, S. L. Lee, H. Keller, J. Blatter, P. H. Kes, and T. W. Li, Phys. Rev. B **54**, 6129 (1996).

[9] W. S. Seow, R. A. Doyle, A. M. Campbell, G. Balakrishnan, K. Kadowaki, and G. Wirth, Phys. Rev. B **53**, 14 611 (1996).

[10] R. Doyle, W. S. Seow, Y. Yan, A. M. Campbell, T. Mochiku, K. Kadowaki, and G. Wirth, Phys. Rev. Lett. **77**, 1155 (1996).

[11] M. Sato, T. Shibauchi, S. Ooi, T. Tamegai, and M. Konczykowski, Phys. Rev. Lett. **79**, 3759 (1997).

[12] M. Kosugi, Y. Matsuda, M. B. Gaifullin, L. N. Bulaevskii, N. Chikumoto, M. Konczykowski, J. Shimoyama, K. Kishio, K. Hirata, and K. Kumagai, Phys. Rev. Lett. **79**, 3763 (1997).

[13] N. Chikumoto, M. Kosugi, Y. Matsuda, M. Konczykowski, and

K. Kishio, Phys. Rev. B **57**, 14 507 (1998).

[14] A. Wahl, V. Hardy, J. Provost, C. Simon, and A. Buzdin, Physica C **250**, 163 (1995).

[15] C. J. van der Beek, M. Konczykowski, T. W. Li, P. H. Kes, and W. Benoit, Phys. Rev. B **54**, R792 (1996).

[16] Qiang Li, Y. Fukumoto, Y. M. Zhu, M. Suenaga, T. Kaneko, K. Sato, and Ch. Simon, Phys. Rev. B **54**, R788 (1996).

[17] R. J. Drost, C. J. van der Beek, J. A. Heijn, M. Konczykowski, and P. H. Kes, Phys. Rev. B **58**, R615 (1998).

[18] R. J. Drost, C. J. van der Beek, H. W. Zandbergen, M. Konczykowski, A. A. Menovsky, and P. H. Kes, Phys. Rev. B **60**, 13 612 (1998).

[19] P. H. Kes, J. Aarts, V. M. Vinokur, and C. J. van der Beek, Phys. Rev. Lett. **64**, 1063 (1990).

[20] J. R. Clem, Phys. Rev. B **43**, 7837 (1991).

[21] D. R. Nelson and V. M. Vinokur, Phys. Rev. Lett. **68**, 2398 (1992); Phys. Rev. B **48**, 13 060 (1993).

[22] Y. Iye, T. Tamegai, and S. Nakamura, Physica C **174**, 227 (1991).

[23] H. Raffy, S. Labdi, O. Laborde, and P. Monceau, Phys. Rev. Lett. **66**, 2515 (1991).

[24] J. C. Martinez, S. Brongersma, A. Koshelev, B. Ivlev, P. H. Kes, R. P. Griessen, D. G. de Groot, Z. Tarnavski, and A. A. Menovsky, Phys. Rev. Lett. **69**, 2276 (1992).

[25] Y. Matsuda, M. B. Gaifullin, K. Kumagai, K. Kadowaki, and T. Mochiku, Phys. Rev. Lett. **75**, 4512 (1995).

[26] N. Morozov, M. P. Maley, L. N. Bulaevskii, and J. Sarrao, Phys. Rev. B **57**, R8146 (1998).

[27] N. Morozov, M. P. Maley, L. N. Bulaevskii, V. Thorsmølle, A. E. Koshelev, A. Petrean, and W. K. Kwok, Phys. Rev. Lett. **82**, 1008 (1999).

[28] T. Hanaguri, Y. Tsuchiya, S. Sakamoto, A. Maeda, and D. G. Steel, Phys. Rev. Lett. **78**, 3177 (1997).

[29] M. Kosugi, Y. Matsuda, M. B. Gaifullin, L. N. Bulaevskii, N. Chikumoto, M. Konczykowski, J. Shimoyama, K. Kishio, and K. Hirata, Phys. Rev. B **59**, 8970 (1999).

[30] L. N. Bulaevskii, M. P. Maley, and V. M. Vinokur, Phys. Rev. B **57**, R5626 (1998).

[31] C. Wengel and U. C. Täuber, Phys. Rev. Lett. **78**, 4845 (1997); Phys. Rev. B **58**, 6565 (1998).

[32] V. Hardy, S. Hébert, M. Hervieu, Ch. Simon, J. Provost, A. Wahl, and A. Ruyter, Phys. Rev. B **58**, 15 218 (1998).

[33] T. W. Li, P. H. Kes, N. T. Hien, J. J. M. Franse, and A. A. Menovsky, J. Cryst. Growth **135**, 481 (1994).

[34] N. Motohira, K. Kuwahara, T. Hasegawa, K. Kishio, and K. Kitazawa, J. Ceram. Soc. Jpn. **97**, 994 (1989).

[35] J. Gilchrist and M. Konczykowski, Physica C **212**, 43 (1993).

[36] C. J. van der Beek, M. Konczykowski, V. M. Vinokur, T. W. Li, P. H. Kes, and G. W. Crabtree, Phys. Rev. B **51**, 15 492 (1995).

[37] A. K. Pradhan, S. B. Roy, P. Chaddah, C. Chen, and B. M. Wanklyn, Phys. Rev. B **52**, 6215 (1995).

[38] This is the same crystal as that used in Ref. 15, Fig. 1.

[39] Z. Hao and J. R. Clem, Phys. Rev. Lett. **67**, 2371 (1991).

[40] A. E. Koshelev, Phys. Rev. B **50**, 506 (1994).

[41] T. W. Li *et al.*, Physica C **257**, 179 (1996).

[42] V. G. Kogan, M. Ledvij, A. Yu. Simonov, J. H. Cho, and D. C. Johnston, Phys. Rev. Lett. **70**, 1870 (1993).

[43] L. N. Bulaevskii, M. Ledvij, and V. G. Kogan, Phys. Rev. Lett. **68**, 3773 (1992).

[44] L. N. Bulaevskii, V. M. Vinokur, and M. P. Maley, Phys. Rev. Lett. **77**, 936 (1996).

[45] G. S. Mkrtchyan and V. V. Shmidt, Zh. Éksp. Teor. Fiz. **61**, 367 (1971) [Sov. Phys. JETP **34**, 195 (1972)].

[46] A. I. Buzdin and D. Feinberg, Physica C **235-240**, 2755 (1994).

[47] R. Ikeda and T. Tsuneto, J. Phys. Soc. Jpn. **60**, 1337 (1991); R. Ikeda, *ibid.* **64**, 1683 (1995).

[48] Z. Tešanović *et al.*, Phys. Rev. Lett. **69**, 3563 (1992).

[49] P. H. Kes, C. J. van der Beek, M. P. Maley, M. E. McHenry, D. A. Huse, M. J. V. Menken, and A. A. Menovsky, Phys. Rev. Lett. **67**, 2383 (1991).

[50] Qiang Li, K. Shibutani, M. Suenaga, I. Shigaki, and R. Ogawa, Phys. Rev. B **48**, 9877 (1993).

[51] We are indebted to Professor J. Blatter for this estimate. A similar estimate can be found in Ref. 52. However, the latter is inapplicable because it describes the situation where pancakes vortices are weakly localized on the columnar defects. Experimentally, we find that thermal wandering of vortices trapped on a columnar defect can be neglected.

[52] A. E. Koshelev, P. LeDoussal, and V. M. Vinokur, Phys. Rev. B **53**, R8855 (1996).

[53] For the lowest matching fields (e.g., 0.2 T) difficulties arise again because the low-field limit of M_{rev} lies entirely within the irreversible regime.

[54] This is the same sample as in Refs. 17 and 18.

[55] C. J. van der Beek, M. Konczykowski, A. V. Samoilov, N. Chikumoto, S. Bouffard, and M. V. Feigel'man (unpublished).

[56] This is the same crystal as in Ref. 15, Figs. 2 and 3.

[57] R. Sugano, T. Onogi, K. Hirata, and M. Tachiki, Phys. Rev. Lett. **80**, 2925 (1998).

[58] C. J. van der Beek and P. H. Kes, Phys. Rev. B **43**, 13 032 (1991).

[59] D. E. Farrell, S. Bonham, J. Foster, Y. C. Chang, P. Z. Jiang, K. G. Vandervoort, D. J. Lam, and V. G. Kogan, Phys. Rev. Lett. **63**, 782 (1990).

[60] Although Ref. 27 states that vortex interactions determine the positional correlations in the vortex liquid, it cannot make statements about which kind of vortex interaction: intralayer repulsion or interlayer attraction.

[61] M. Konczykowski, Physica C **235-240**, 197 (1994); M. Konczykowski, N. Chikumoto, V. Vinokur, and M. Feigel'man, *ibid.* **235-240**, 2845 (1994).